ELSEVIER

Journal of Alloys and Compounds 446–447 (2007) 84–89

Journal of ALLOYS AND COMPOUNDS

www.elsevier.com/locate/jallcom

Enhanced hydrogen reaction kinetics of nanostructured Mg-based composites with nanoparticle metal catalysts dispersed on supports

Yeong Yoo [a,*], Mark Tuck [b], Rajender Kondakindi [a], Chan-Yeol Seo [a], Zahir Dehouche [c], Khaled Belkacemi [c]

[a] *Institute for Chemical Process and Environmental Technology, National Research Council Canada, Ottawa, Ontario K1A 0R6, Canada*
[b] *Department of Chemical Engineering, Dalhousie University, Halifax, Nova Scotia B3J 2X4, Canada*
[c] *Department of Soil Sciences and Agri-Food Engineering, Laval University, Quebec City, Quebec G1K 7P4, Canada*

Received 29 October 2006; received in revised form 12 December 2006; accepted 13 December 2006
Available online 21 December 2006

Abstract

Hydrogen reaction kinetics of nanocrystalline MgH_2 co-catalyzed with $Ba_3(Ca_{1+x}Nb_{2-x})O_{9-\delta}$ (BCN) proton conductive ceramics and nanoparticle bimetallic catalyst of Ni/Pd dispersed on single wall carbon nanotubes (SWNTs) support has been investigated. The nanoparticle bimetallic catalysts of Ni/Pd supported by SWNTs were synthesized based on a novel polyol method using $NiCl_2{\cdot}6H_2O$, $PdCl_2$, NaOH and ethylene glycol (EG). The nanostructured Mg composites co-catalyzed with BCN and bimetallic supported catalysts exhibited stable hydrogen desorption capacity of 6.3–6.7 wt.% H_2 and the significant enhancement of hydrogen desorption kinetics at 230–300 °C in comparison to either non-catalyzed MgH_2 or the nanocomposite of MgH_2 catalyzed with BCN.

Keywords: Hydrogen storage materials; Polyol method; Ni/Pd nanoparticle catalyst; Magnesium hydride; Proton conductive ceramic catalyst

1. Introduction

Magnesium hydride having a high hydrogen storage capacity of 7.6 wt.% is considered as one of the most interesting alternatives for the reversible storage of hydrogen. However, the major problem of magnesium as a rechargeable hydrogen carrier system is its slow reaction rate and high sorption temperature. To overcome this problem, metallic catalysts such as Pd, Ni, V, Ti, Mn and Fe have been added to nanocrystalline magnesium for a better H_2-dissociation at the surface [1,2]. Recently Hanada et al. have reported the catalytic effect of nanoparticle Ni on hydrogen storage properties of MgH_2 [3,4]. The nanosized Ni doping significantly decreased the activation energy for hydrogen desorption by surface activation, resulting in 90% of hydrogen desorption within 100 min at 163 °C. Kojima et al. have reported that nanocomposite MgH_2 catalyzed with nano-Ni/Al_2O_3/C desorbed 4.9–5.8 wt.% H_2 at 423–473 K [5]. Gutfleisch et al. have reported that hydrogen desorption temperature is reduced significantly to less than 140 °C when MgH_2 is co-milled with 0.5 wt.% $PdOH_2O$ and 5 at.% or 10 at.% Ni [6]. In addition, Gutfleisch et al. have also reported a Mg–1 wt.% Ni–0.2 wt.% Pd alloy produced via induction melting with consequent reactive milling exhibited 41 kJ/mol for absorption and 110 kJ/mol for the desorption reaction, indicating excellent hydrogen absorption/desorption kinetics [7]. Therefore, nano-Ni/Pd catalyst uniformly dispersed on nanocrystalline MgH_2 can be considered to exhibit very attractive catalytic effect on enhancing hydrogen sorption kinetics.

In another approach, transition metal oxides such as TiO_2, V_2O_5, CuO, Mn_2O_3, Cr_2O_3, Fe_3O_4, and Nb_2O_5, etc. have been investigated as potential catalysts on the sorption behavior of nanocrystalline Mg-based systems [3,8]. Recently, Yoo et al. have reported the catalytic effect of proton conductive ceramics on enhancing hydrogen desorption kinetics of nanostructured magnesium hydrides [9,10]. After milling MgH_2–$Ba_3(Ca_{1+x}Nb_{2-x})O_{9-\delta}$ (BCN) composite, the nanostructured composite showed much enhanced desorption kinetics, increased desorption plateau pressure, and decreased hysteresis, $\ln(P_{abs}/P_{des})$, indicating not only ameliorate desorption kinetics but also lower temperature desorption in comparison to pure MgH_2.

* Corresponding author. Tel.: +1 613 993 5331; fax: +1 613 991 2384.
E-mail address: yeong.yoo@nrc-cnrc.gc.ca (Y. Yoo).

0925-8388/$ – see front matter.
doi:10.1016/j.jallcom.2006.12.054

Therefore, in this work, the hydrogen reaction kinetics of nanocrystalline MgH_2 co-catalyzed with $Ba_3(Ca_{1+x}Nb_{2-x})O_{9-\delta}$ (BCN) proton conductive ceramics and nanoparticle bimetallic catalysts of Ni/Pd dispersed on single wall carbon nanotubes (SWNTs) support has been investigated.

2. Experimental procedures

Magnesium hydride (MgH_2) powder was purchased from Alfa-Aesar (98% purity) and mechanically milled under argon by using a Spex 8000 high energy mill for 18 h to prepare nanostructured MgH_2. The ball to powder ratio was 10:1.

BCN catalyst ($Ba_3(Ca_{1+x}Nb_{2-x})O_{9-\delta}$, $x = 0$) [11] was prepared from polymeric precursors by the Pechini method [12]. The starting materials of barium carbonate dissolved in nitric acid solution, calcium carbonate dissolved in nitric acid solution, and ammonium citric solution converted from ammonium niobate oxalate hydrate were mixed with a stoichiometric amount of citric acid. The resulting solution was stirred for about 1 h on a hot plate and the temperature was stabilized at 70 °C. The mixture was heated to 90 °C, at which point ethylene glycol was added at a mass ratio of 40:60 with respect to citric acid. The temperature was maintained constant at 160 °C for resin formation and thermal decomposition. The precursor powders were then calcined at 700 °C for 4 h and again heat-treated at 1000 °C for 1 h as the final step for the synthesis of BCN single phase.

The nanoparticle Ni/Pd catalysts (Ni:Pd = 10:1 and 2:1 in molar ratio) supported on SWNTs (Ni/Pd:SWNT = 1:1 weight ratio) also having catalytic effect on enhancing kinetics of hydrogen storage materials were prepared based on a novel polyol method developed by Bock et al. [13] for preparing Pt/Ru nanoparticles. In this method, precursor salts of $NiCl_2{\cdot}6H_2O$ (Sigma–Aldrich, PeagentPlus) and $PdCl_2$ (Sigma–Aldrich, 99.9%) were dissolved in ethylene glycol containing 0.2 M NaOH. The solutions were stirred for 30 min in air at room temperature, subsequently heated under reflux to 160 °C for 3 h, and then cooled in air. Appropriate aliquots of the colloidal solutions were mixed with single wall carbon nanotubes (Microtechnano, SWNTs purity 92 wt.%, amorphous carbon 6 wt.%, ash 2 wt.%, surface area 640 m^2/g) in a large and open beaker for up to 24 h, resulting in the deposition of the Ni/Pd colloids on the SWNTs. The SWNTs-supported Ni/Pd catalysts were then filtered, washed with water, and dried at 100 °C in air for 1 h.

The nanocrystalline composites of MgH_2 containing BCN catalyst were prepared by milling a mixture of 18 h milled MgH_2 and 2 wt.% of BCN for additional 2 h. The final co-catalyzed MgH_2 nanocomposites containing the supported Ni/Pd catalysts as well as BCN were prepared by milling a mixture of the milled MgH_2–BCN composite and the SWNTs-supported Ni/Pd catalysts for additional 20 min.

Thermodynamics and kinetics of the nanostructured MgH_2 composites were determined by a Sievert-type sorption analyzer (Hy-Energy, PCT Pro2000). The surface morphology, microstructure, surface oxidation state and phase of the as-milled MgH_2 and the supported catalysts were determined by using scanning electron microscopy (SEM), transmission electron microscopy (TEM), X-ray photoelectron spectroscopy (XPS) and X-ray diffraction on a Bruker's D8 Diffractometer. The crystallite size was also obtained by a TOPAS program (Bruker). The dehydrogenation behavior of the nanocomposites with catalysts was studied by differential scanning calorimetry (DSC 2920, TA instruments). The milled nanocomposite sample of 4 mg was placed in an aluminum pan, and a lid was crimped onto the pan in dry box filled with argon. The pan was then placed in the sample cell of the DSC module. The temperature of the DSC module was equilibrated at 50 °C and then increased at a rate of 1–20 °C/min under a N_2 gas purge up to 500 °C.

3. Results and discussion

3.1. Structural characterization of mechanically milled MgH_2 and synthesized catalysts

Fig. 1 shows the X-ray diffraction patterns of the composites: (a) pure MgH_2 as received, (b) MgH_2 milled for 18 h, (c) synthesized BCN catalyst and (d) MgH_2–2 wt.% BCN nanocomposite milled for additional 2 h. As shown in Fig. 1(a) and (b), the high energy milling of as-received MgH_2 for 18 h increased the diffraction peak line widths, indicating that the high energy milling reduced the average crystallite size present in the original β-MgH_2 material and/or increased its microstructural strain, and induced the phase transformation from β-MgH_2 to the nanocrystalline mixture phases of β-MgH_2 tetragonal phase and γ-MgH_2 orthorhombic phase. Fig. 1(c) shows a well crystallized cubic perovskite structure of BCN single phase. As shown in Fig. 1(d), the additional milling of the mixture of 18 h milled MgH_2 and BCN catalyst for 2 h kept the BCN phase, indicating that the proton conductor exists on the surface of MgH_2 particles and that surface inter-diffusion between MgH_2 and BCN may cause the formation of Ba, Ca and Nb-rich reacted zone as hydroxides or even hydrides on the surface of MgH_2 as described in Ref. [10].

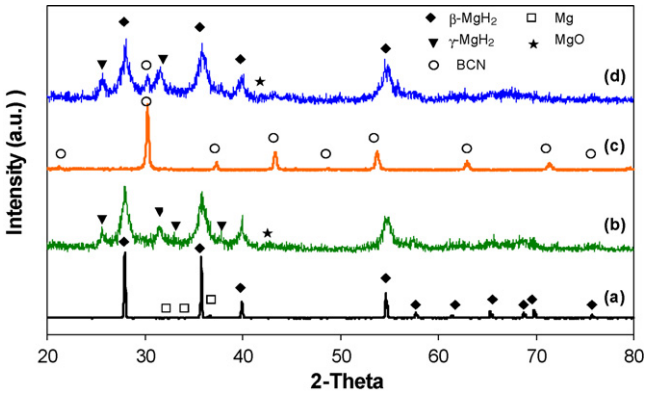

Fig. 1. X-ray diffraction patterns of the composites: (a) pure MgH_2 as received, (b) MgH_2 milled for 18 h, (c) BCN catalyst and (d) MgH_2–2 wt.% BCN nanocomposite milled for additional 2 h.

SWNTs-supported Ni/Pd catalysts having two different molar ratios of Ni/Pd = 10/1 and 2/1 were synthesized by the polyol method using ethylene glycol (EG)–NaOH. As for a supporting material for the deposition of metal nanocatalysts, SWNTs was used because it was reported that SWNTs can act as catalysts to improve the hydrogen absorption and desorption properties of metallic catalyst-doped hydrides [14,15]. It was also reported that the nanotube length decreases with increasing ball milling time [16]. In order to prevent the thorough destruction of SWNTs during the high energy milling, a short milling time of 20 min was applied for mixing the milled MgH_2–BCN composite and the SWNTs-supported Ni/Pd catalysts in this study. However, it should be noted that the high surface area carbon as a supporting material may provide a similar beneficial effect on enhancing hydrogen sorption kinetics and the direct observation of SWNTs in the milled composites as a function of milling time has to be done to confirm the effect of mechanically milled SWNTs in the composites.

Ethylene glycol is an alcohol and is readily oxidized to act as a reducing agent for the Ni and Pd precursor salts. The detailed suggested mechanism was described in literature [13]. The addition of NaOH into the EG system accelerates the reduction of metal ions to metal nanoparticles even at room tempera-

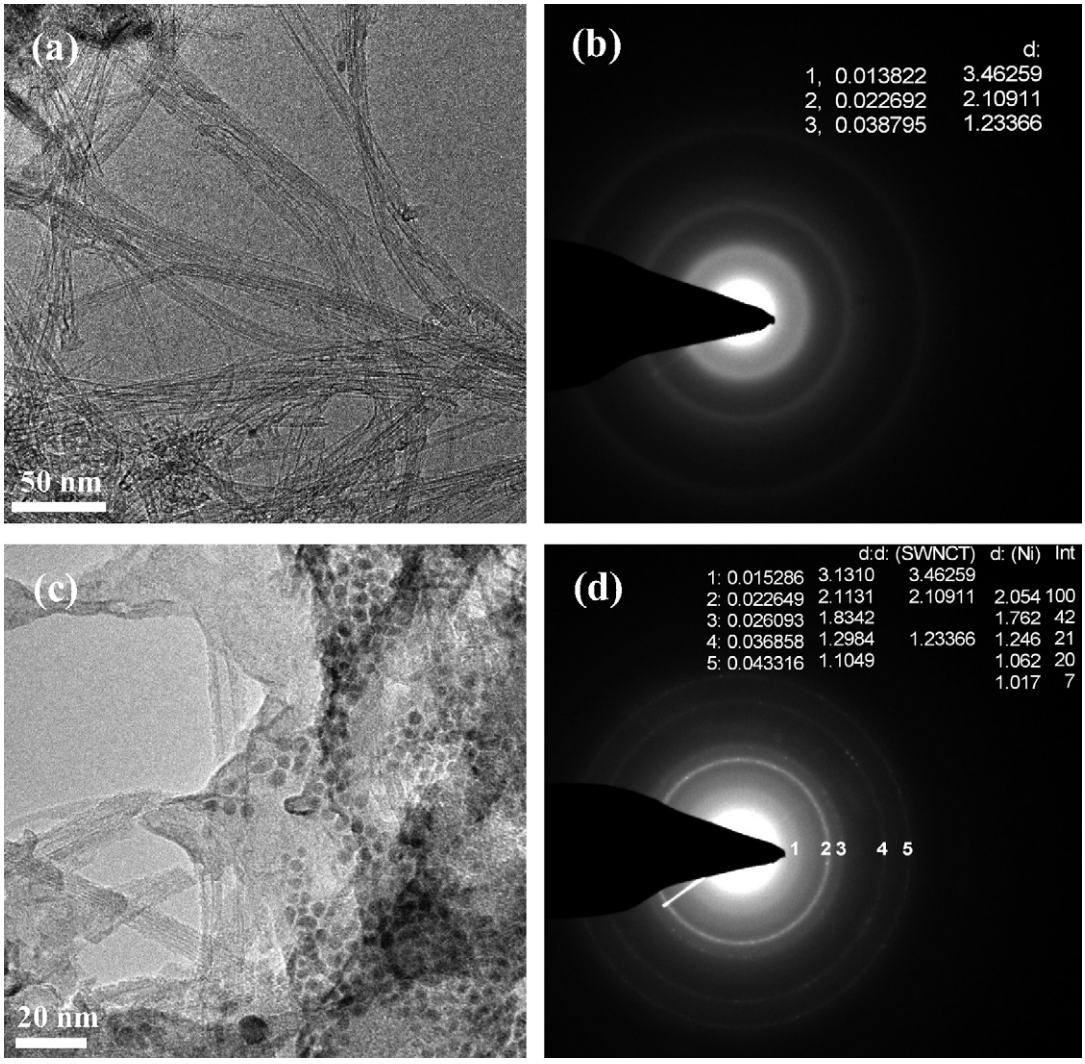

Fig. 2. Transmission electron micrographs and electron diffraction patterns of (a) and (b) SWNT and (c) and (d) supported Ni catalysts.

ture without the need for external reducing agent and decreases the particle size [17]. The formation of Ni metal nanoparticles by chemical method is known to be very difficult because nickel is easily oxidized [18]. The X-ray diffraction patterns and XPS spectra of SWNTs-supported Ni/Pd catalysts prepared in ethylene glycol (EG)–NaOH solution without using poly(*N*-vinyl-2-pyrrolidone) (PVP) as a stabilizing agent revealed the difficulty in preparing fully homogenous bimetallic Ni/Pd alloy and preventing the formation of NiO on the surface of Ni nanoparticles. Shifted Ni and pure Pd metallic phases in the X-ray diffraction patterns and NiO related small peaks at 855.5 eV as well as Ni and Pd at 853.7 and 335.9 eV, respectively, in XPS spectra were observed. It was reported that even if two monolayers of NiO are formed on the Ni surface, the intensity of the Ni^{2+} (2p) peak is greater than the Ni^{0} (2p) peak [19]. Therefore, the extent of oxidation of Ni is not significant and the oxidation may be due to oxygen associated with EG absorbed on the Ni particles and hydroxide formation on the Ni surface during filtering and washing with water. The mixing of Pd salt with Ni salt was very effective to reduce the Ni^{2+} ions with ethylene glycol because the solution showed very fast color change from yellow to dark brown during refluxing. It was reported that the Ni^{2+} ions are thought to be reduced at the surface of the Pd nanoparticles, presumably on the most catalytically active {1 1 1} surface [20].

Fig. 2 shows the TEM images and corresponding electron diffraction patterns of SWNTs and supported Ni catalysts. The particles essentially were monodispersed with an average diameter of 5.0–7.0 nm, consistent with the crystallite size of 5.6 nm calculated by calculated by TOPAS program from X-ray diffraction patterns. Five fringe patterns with plane distances of 3.13, 2.11, 1.83, 1.29, and 1.10 Å could be observed from Ni nanoparticle catalysts on SWNTs and four fringe patterns (nos. 2–5) except for the first pattern related to SWNTs were consistent with the indices (1 1 1), (2 0 0), (2 2 0), and (3 1 1) of pure face-centered cubic (fcc) nickel as shown in Fig. 2d.

3.2. Dehydrogenation behavior of the milled nanocrystalline composites of MgH_2 containing different catalysts

Fig. 3 shows DSC curves of the as received and as-milled samples with or without catalysts at a heating rate of 5 °C/min.

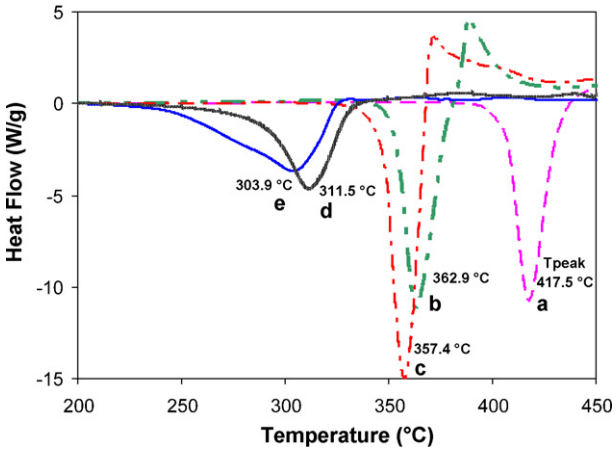

Fig. 3. DSC curves of (a) as-received MgH_2, (b) 18 h milled MgH_2, (c) MgH_2–BCN composite, (d) MgH_2–BCN–Ni/Pd(=2/1)/SWNTs composite and (e) MgH_2–BCN–Ni/Pd(=10/1)/SWNTs composite, at a heating rate of 5 °C/min.

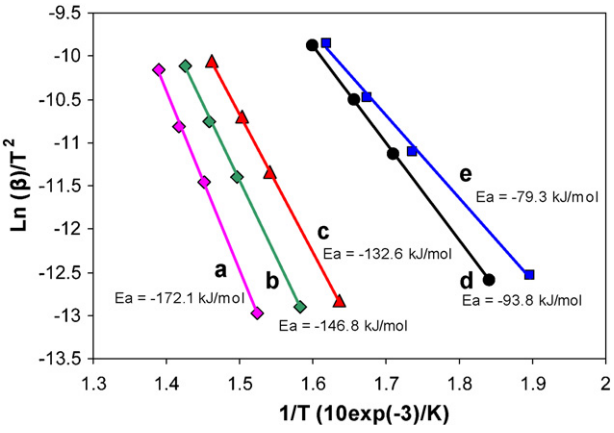

Fig. 4. Kissinger plots of the hydrogen desorption reaction of (a) as-received MgH_2, (b) 18 h milled MgH_2, (c) MgH_2–BCN composite, (d) MgH_2–BCN–Ni/Pd(=2/1)/SWNTs composite and (e) MgH_2–BCN–Ni/Pd(=10/1)/SWNTs composite at various heating rates (β = 1, 5, 10, and 20 °C/min).

The endothermic peaks correspond to the decomposition of the hydrides phases. The nanostructured MgH_2 milled for 18 h has a hydrogen desorption peak around 363 °C, which is much lower than that of as received MgH_2 (417.5 °C). Thus, the reduction of crystallite size was very effective to decrease the decomposition temperature. The BCN doping to milled MgH_2 further decreased the decomposition temperature and increased the heat flow in comparison to non-catalyzed MgH_2, potentially resulting in the increase of the enthalpies of formation. The additional milling of the mixture of 2 wt.% of BCN and milled MgH_2 may cause the formation of Ba and Ca hydrides or hydroxides or (Mg, M)H_x (M = Ba, Ca) in addition to Nb–H_x at the interface which can act as the enhanced path for hydrogen diffusion or active sites for hydrogen dissociation and recombination. However, the enthalpies of formation of BaH_2 and CaH_2 are 86 and 94 kJ/mol H_2, respectively, and higher than that of MgH_2 (71 kJ/mol H_2) [21]. In addition, the decomposition temperatures of BaH_2 and CaH_2 are 675 and 600 °C, respectively, and much higher than that of MgH_2 (327 °C) [22]. There are many ternary hydrides such as Ba_2MgH_6, $BaMgH_4$, $Ba_6Mg_7H_{26}$, $Ba_2Mg_3H_{10}$, and $Ca_4Mg_3H_{14}$ that can be formed at the interface and have undefined values of the decomposition temperature and enthalpies of formation. Therefore, it is very difficult to determine the interfacial phases that cannot be detected by X-ray diffraction analysis. The kinetics of hydrogen sorption should be investigated for evaluating the effectiveness of BCN doping and is described in the next section. The further addition of 2 wt.% of Ni–Pd nanocatalysts on SWNTs into BCN-doped MgH_2 decreased the peak decomposition temperature to about 310 °C and broadened DSC profile in the temperature range from 340 to 220 °C. The Ni-rich nanocatalyst-added MgH_2 composite exhibited the most superior catalytic effect among all composites tested in this work and asymmetrical endothermic peaks having the low temperature peak related to the desorption from γ-MgH_2 and some amount of β-MgH_2 [23].

Fig. 4 shows Kissinger plot of the hydrogen desorption reaction for catalyzed MgH_2 samples at various heating rates (β = 1, 5, 10, and 20 °C/min). The apparent activation energy for hydrogen desorption can be estimated by the Kissinger method [24] from DSC curves using the following equation:

$$\ln\left(\frac{\beta}{T_p^2}\right) = -\frac{E_a}{RT_p} + \alpha \quad (1)$$

where β is the heating rate, T_p the peak temperature, E_a the apparent activation energy, R the gas constant, and α is the linear constant.

From the slope of these straight lines, the activation energies of as received MgH_2 and 18 h milled MgH_2 were estimated to be 172.1 and 146.8 kJ/mol, respectively, similar to the reported values (156 and 144 kJ/mol) [25,5]. Even though BCN catalyst was very effective to enhance desorption kinetics at 300 °C [9,10], Ni/Pd metallic catalysts were much effective to enhance sorption kinetics at lower temperature according to DSC data. Ni-rich nanocatalyst-added MgH_2 composite exhibited the low activation energy of 79.3 kJ/mol, corresponding to the reported values (88.1 and 74 kJ/mol) [2,5].

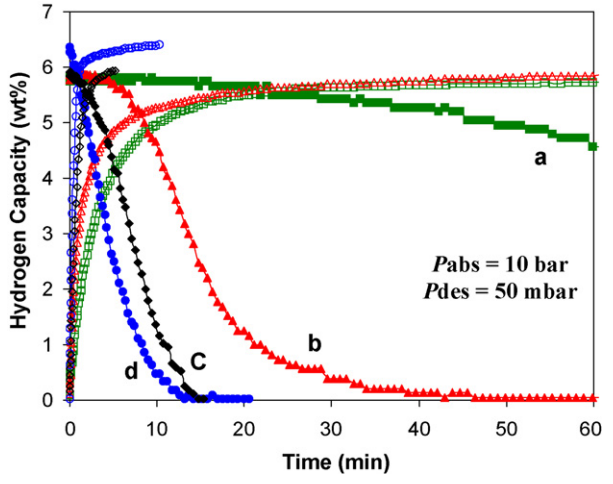

Fig. 5. Hydrogen absorption and desorption curves of (a) 18 h milled MgH_2, (b) MgH_2–BCN composite, (c) MgH_2–BCN–Ni/Pd(=2/1)/SWNTs composite and (d) MgH_2–BCN–Ni/Pd(=10/1)/SWNTs composite at 300 °C.

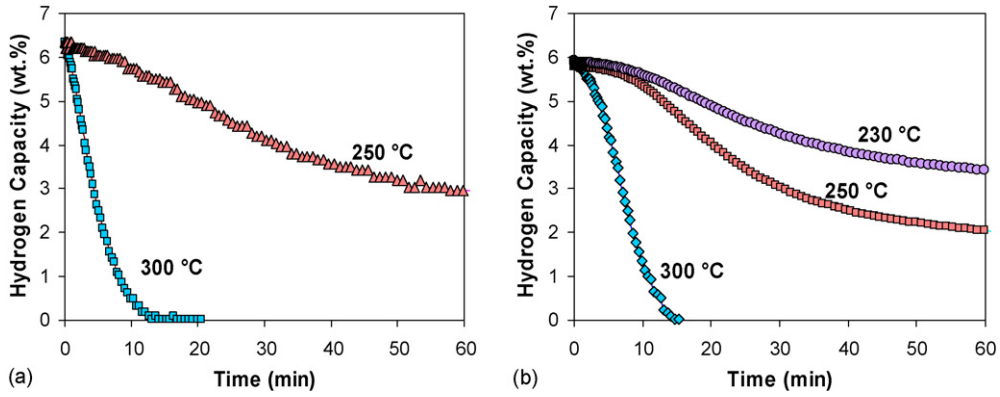

Fig. 6. Hydrogen desorption curves of (a) MgH_2–BCN–Ni/Pd(=10/1)/SWNTs composite, and (b) MgH_2–BCN–Ni/Pd(=2/1)/SWNTs composite under an initial hydrogen pressure of 50 mbar at different temperatures.

3.3. Hydrogen sorption properties

Fig. 5 shows the hydrogen absorption and desorption curves of the composites. The Ni-rich (Ni/Pd = 10/1) nanocatalyst-added MgH_2 composite exhibited the best absorption and desorption kinetics at 300 °C, corresponding to the apparent activation energies of hydrogen desorption determined by DSC. Ni has a comparatively high 3d orbital occupancy. Therefore, occupied state is dominant with respect to the 3d orbital. This largely contributes to the back-donation of the electrons to the antibonding orbitals of MgH_2, resulting in the easier Mg–H dissociation [26].

Fig. 6 shows the hydrogen desorption curves of (a) MgH_2–BCN–Ni/Pd(=10/1)/SWNTs composite, and (b) MgH_2–BCN–Ni/Pd(=2/1)/SWNTs composite under an initial hydrogen pressure of 50 mbar at 230, 250 and 300 °C. It can be seen that both of catalysts are not sufficient to provide fast kinetics and high hydrogen capacity at 230 and 250 °C, even if DSC data of catalyzed MgH_2 are quite promising to enhance sorption behavior at low temperature. Therefore, the effect of the concentration of catalysts on enhancing desorption kinetics at low temperature should be further investigated.

The PCI (pressure–composition-isotherms) curves at 300 °C for nanostructured MgH_2 composites with different catalysts are shown in Fig. 7. The various catalyst-containing MgH_2 composites exhibited high maximum hydrogen absorption capacities, $(H/M)_{max}$ in the range of 6.3–6.7 wt.%. The equilibrium pressures of H-desorption and reversible hydrogen absorption–desorption capacities for catalyzed MgH_2 increased significantly in comparison to non-catalyzed MgH_2. The hysteresis, $\ln(P_{abs}/P_{des})$, of catalyzed MgH_2 during hydrogen absorption and desorption was much smaller than non-catalyzed MgH_2 due to the decreased mechanical stress between the metal and the hydride phases or the reduced kinetic constraints during the measurement [27].

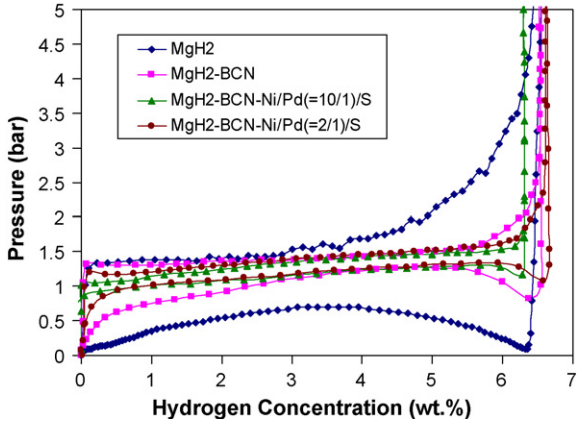

Fig. 7. PCI curves at 300 °C for nanostructured MgH_2 composites with different catalysts.

4. Conclusions

Nanocrystalline MgH_2 composites co-catalyzed with $Ba_3(Ca_{1+x}Nb_{2-x})O_{9-\delta}$ (BCN) proton conductive ceramics and nanoparticle bimetallic catalyst of Ni/Pd dispersed on single wall carbon nanotubes (SWNTs) support have been successfully prepared by a consecutive combination of Pechini process, novel polyol method, and three step high energy milling. The apparent activation energies for the hydrogen desorption of MgH_2 nanocomposites with or without catalysts were determined by the Kissinger method from DSC curves. The Ni-rich (Ni/Pd = 10/1) nanocatalyst-added MgH_2 composite exhibited the fastest absorption and desorption kinetics at 300 °C, but 2 wt.% addition of SWNTs-supported Ni/Pd catalysts was not enough to provide fast kinetics and high hydrogen capacity at 230 and 250 °C. The maximum hydrogen absorption capacities of nanostructured MgH_2 composites co-catalyzed with BCN and bimetallic supported catalysts, $(H/M)_{max}$ in the range of 6.3–6.7 wt.% were obtained by PCI (pressure–composition-isotherms) curves at 300 °C. The nanostructured Mg composites co-catalyzed with BCN and bimetallic supported catalysts exhibited the significant enhancement of hydrogen desorption kinetics at 230–300 °C in comparison to either non-catalyzed MgH_2 or the nanocomposite of MgH_2 catalyzed with BCN.

Acknowledgements

This work was supported by Program of Energy Research and Development (PERD) Technology and Innovation (T&I)

in Canada. The authors gratefully acknowledge the help of Mr. Dashan Wang for TEM, Mr. David Kingston for XPS, Mr. Nguon Lim for DSC and Dr. Patrick Mercier for XRD data analysis.

References

[1] L. Zaluski, A. Zaluska, P. Tessier, J.O. Strom-Olsen, R. Schulz, J. Alloys Compd. 217 (1995) 295.
[2] G. Liang, J. Huot, S. Boily, A. Van Neste, R. Schulz, J. Alloys Compd. 292 (1999) 247.
[3] N. Hanada, T. Ichikawa, H. Fuji, J. Alloys Compd. 404–406 (2005) 716–719.
[4] N. Hanada, T. Ichikawa, H. Fuji, J. Phys. Chem. B 109 (2005) 7188–7194.
[5] Y. Kojima, Y. Kawai, T. Haga, J. Alloys Compd. 424 (2006) 294.
[6] O. Gutfleisch, N. Schlorke-de Boer, N. Ismail, M. Herrich, A. Walton, J. Speight, I.R. Harris, A.S. Pratt, A. Zuttel, J. Alloys Compd. 356–357 (2003) 598.
[7] O. Gutfleisch, S. Dal Toe, M. Herrich, A. Handstein, A. Pratt, J. Alloys Compd. 404–406 (2005) 413.
[8] W. Oelerich, T. Klassen, R. Bormann, J. Alloys Compd. 315 (2001) 237.
[9] Y. Yoo, Z. Dehouche, C. Seo, I. Davidson, N. Grimard, J. Goyette, International Partnership Hydrogen Economy Hydrogen Storage Conference, Lucca, Italy, June 2005.
[10] C. Seo, Y. Yoo, Z. Dehouche, Proceedings of the International Hydrogen Energy Congress and Exhibition, Istanbul, Turkey, 2005, p. 35.
[11] T. Schober, J. Friedrich, Solid State Ionics 136–137 (2000) 161.
[12] M.P. Pechini, US Patent 3,330,697 (1967).
[13] C. Bock, C. Paquet, M. Couillard, G.A. Botton, B.R. MacDougall, J. Am. Chem. Soc. 126 (2004) 8028–8037.
[14] Z. Dehouche, L. Lafi, N. Grimard, J. Goyette, R. Chahine, Nanotechnology 16 (2005) 402.
[15] C. Wu, P. Wang, X. Yao, C. Liu, D. Chen, G.Q. Lu, H. Cheng, J. Phys. Chem. B 109 (2005) 22217.
[16] N. Pierard, A. Fonseca, Z. Konya, I. Willems, G. Van Tendeloo, J.B. Nagy, Chem. Phys. Lett. 335 (2001) 1.
[17] L.J. Chen, C.C. Wan, Y.Y. Wang, J. Colloid Interf. Sci. 297 (2006) 143.
[18] D.H. Chen, C.H. Hsieh, J. Mater. Chem. 12 (2002) 2412.
[19] K. Nagaveni, A. Gayen, G.N. Subbanna, M.S. Hedge, J. Mater. Chem. 12 (2002) 3147.
[20] T. Teranish, M. Miyake, Chem. Mater. 11 (1999) 3414.
[21] A. Krozer, A. Fisher, L. Schlapbach, Phys. Rev. B 53 (20) (1996) 13808.
[22] W. Grochala, P. Edwards, Chem. Rev. 104 (2004) 1283.
[23] F.C. Gennari, F.J. Castro, G. Urretavizcaya, J. Alloys Compd. 321 (2001) 46.
[24] H.E. Kissinger, Anal. Chem. 29 (1957) 1702.
[25] J. Huot, G. Liang, S. Boily, A. Van Neste, R. Schultz, J. Alloy Compd. 293–295 (1999) 495.
[26] M. Tsuda, W.A. Difio, H. Kasai, H. Nakanishi, H. Aikawa, Thin Solid Films 509 (2006) 157.
[27] T. Spassov, V. Rangelova, P. Solsona, M.D. Baro, D. Zander, U. Koster, J. Alloys Compd. 398 (2005) 139.